nature chemical biology

Monomeric fluorescent timers that change color from blue to red report on cellular trafficking

Fedor V Subach[1,2], Oksana M Subach[1,2], Illia S Gundorov[1], Kateryna S Morozova[1], Kiryl D Piatkevich[1], Ana Maria Cuervo[1] & Vladislav V Verkhusha[1]

Based on the mechanism for chromophore formation in red fluorescent proteins, we developed three mCherry-derived monomeric variants, called fluorescent timers (FTs), that change their fluorescence from the blue to red over time. These variants exhibit distinctive fast, medium and slow blue-to-red chromophore maturation rates that depend on the temperature. At 37 °C, the maxima of the blue fluorescence are observed at 0.25, 1.2 and 9.8 h for the purified fast-FT, medium-FT and slow-FT, respectively. The half-maxima of the red fluorescence are reached at 7.1, 3.9 and 28 h, respectively. The FTs show similar timing behavior in bacteria, insect and mammalian cells. Medium-FT allowed for tracking of the intracellular dynamics of the lysosome-associated membrane protein type 2A (LAMP-2A) and determination of its age in the targeted compartments. The results indicate that LAMP-2A transport through the plasma membrane and early or recycling endosomes to lysosomes is a major pathway for LAMP-2A trafficking.

Monomeric fluorescent proteins of various emission wavelengths have become invaluable tools for studying the spatial behavior of intracellular molecules, including their localization and interaction[1]. To visualize temporal and spatial molecular events, FTs[2], which change their emission wavelengths over time, could be especially valuable. The only currently available FT is DsRed-Timer FT (also known as DsRed-E5)[3]; however, it is a tetramer, which prevents its application as a protein fusion tag. Nevertheless, the tetrameric state of the DsRed-Timer does not limit its use to study gene activities[4], relative age of organelles[5] and cell differentiation[3].

It has been suggested that a red DsRed-like chromophore in the red fluorescent proteins (RFPs) results from an oxidation of a protonated blue form of the GFP-like chromophore, not from the green anionic form, which is a dead-end product[6]. This suggested scheme for red chromophore maturation provides a basis for developing monomeric FTs that change their color from blue to red. The most suitable templates for this appear to be the monomeric variants of DsRed[7]. One of these variants, mCherry, was chosen for a directed molecular evolution to develop three monomeric FTs with different maturation rates between the protonated blue GFP-like and the anionic red DsRed-like chromophore states.

FTs can be used as molecular genetically encoded tools to study trafficking of different cellular proteins and to provide accurate insight into the timing of intracellular processes. The sequence of events during trafficking of different cellular proteins before they reach their final compartment has often been the subject of contradictory investigations. An example of a long-standing dilemma is the contribution of different pathways to trafficking and final delivery of LAMP-2A to lysosomes. LAMP-2A is encoded by a spliced variant of the *lamp2* gene and acts as a lysosomal receptor for chaperone-mediated autophagy (CMA)[8,9]. LAMP-2A is sorted to endosomes and lysosomes through a tyrosine-based signal in its cytosolic C terminus, but a fraction of the protein is also observed at the plasma membrane[10]. This dual location led investigators to propose the existence of both direct (Golgi to lysosomes) and indirect (through endocytosis from the plasma membrane) targeting of LAMP-2A to lysosomes[11]. The use of FTs has allowed us to study the sequence of events involved in transport of LAMP-2A to lysosomes and to determine the preferential pathway followed by LAMP-2A for its trafficking.

RESULTS

Development of monomeric FTs

The gene encoding mCherry was used as a template for the multiple saturated mutagenesis at positions 42, 44, 65, 69, 106, 148, 203 and 224 (amino acid numbering follows that of *Aequorea victoria* GFP; see **Fig. 1a**). These positions were identified either according to the X-ray structure of mCherry[12] or using experimental data regarding amino acid substitutions affecting maturation of DsRed variants[13–15]. It has been shown that substitutions at these positions slow or accelerate formation of the red chromophore. According to the mCherry structure, residues 42 and 44 are close to the Met65 residue of the mCherry chromophore, and residues 69, 148 and 203 are close to the phenolic and/or imidazolinone rings of the chromophore. Residue 224 was found in close proximity to residue 203 and has been suggested to indirectly influence chromophore positioning. Therefore, a bacterial

[1]Department of Anatomy and Structural Biology, and Gruss-Lipper Biophotonics Center, Albert Einstein College of Medicine, 1300 Morris Park Avenue, Bronx, New York 10461, USA. [2]These authors contributed equally to this work. Correspondence should be addressed to V.V.V. (vverkhus@aecom.yu.edu).

Received 30 October 2008; accepted 11 December 2008; published online 11 January 2009; doi:10.1038/nchembio.138

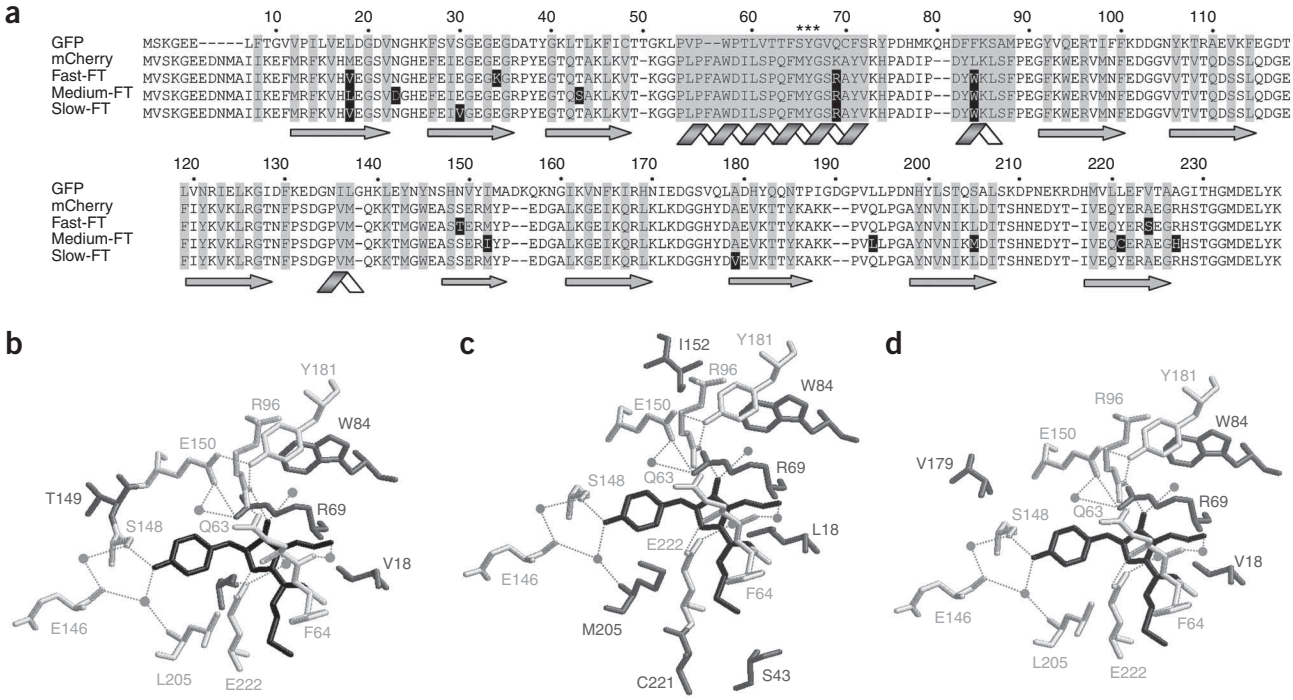

Figure 1 Structural basis of the amino acid substitutions converting mCherry into the FTs. (**a**) Alignment of the amino acid sequences of FTs with GFP and mCherry. Residues buried in β-can are shaded. Stars indicate residues that are forming the chromophore. β-sheet–forming regions and α-helixes are denoted as arrows and ribbons, respectively. Mutations in FTs relative to mCherry are shown in black. Alignment numbering follows that of GFP. (**b**–**d**) Immediate environment of the chromophore in parental mCherry with mutations found in fast-FT (**b**), medium-FT (**c**) and slow-FT (**d**). The surrounding residues are shown within 9.5 Å of the chromophore. The chromophore is shown in black, conserved amino acid residues are in light gray, and mutated residues are in gray. Water molecules are represented as gray spheres. Hydrogen bonds are indicated with dashed gray lines. Substitution of amino acid residues was performed using Swiss PDBViewer v.3.7 (http://www.expasy.org/spdbv/). The best fits for the introduced mutated residues were achieved by selection of the rotamers with the lowest scores.

library of mutants at positions 42, 44, 65, 69, 106, 148, 203 and 224 was screened for clones with fast, medium and slow maturation rates using a fluorescence-activated cell sorter (FACS) followed by analysis of the collected colonies on petri dishes using a fluorescence stereomicroscope.

As a result of screening the library of mutants with the site-specific substitutions at the eight positions indicated above, mCherry K69R and mCherry K69R A224S mutants with FT phenotypes were found (**Supplementary Table 1** online). These mutants exhibited blue forms that were not detected in the original mCherry. However, the brightness of the blue fluorescence was very low in the case of mCherry K69R. The maturation rates of the red forms were slowed as compared to that of mCherry. Other mutations found in the analyzed variants did not lead to the FT phenotypes. Because the mCherry K69R A224S mutant exhibited the blue form earlier than the mCherry K69R variant, the former was further used for random mutagenesis to screen for the fast-FT phenotype. Consequently, the mCherry K69R mutant was used as a template for random mutagenesis aimed to screen for medium-FT and slow-FT phenotypes. Sequential rounds of the random mutagenesis followed by screening of mutant clones using FACS and fluorescence stereomicroscopy were applied. The bacterial libraries of random mutants typically consisted of 10^6 to 10^7 clones.

The number of rounds for random mutagenesis varied depending on the specific FT phenotype and consisted of four, five and three rounds for the fast-FT, medium-FT and slow-FT, respectively. Over several rounds of random mutagenesis, the fluorescence intensities of both blue and red forms of the best FT variants increased and reached plateaus (**Supplementary Fig. 1** online). When we were not able to find a better variant in the next round of mutagenesis, we stopped improvement of that FT using random mutagenesis.

A key mutation found in the first round of mutagenesis for all FT phenotypes was L84W. Variants containing this amino acid substitution exhibited substantially brighter blue and red fluorescence intensities. Mutations at position 18 such as M18V and M18L resulted in a slight decrease of the red intensity that, however, was compensated by a large increase of the blue fluorescence. Therefore we decided to choose variants with these mutations for the next random mutagenesis.

During the subsequent rounds of mutagenesis, several additional internal positions such as 112, 143, 152, 179 and 205, which contained important substitutions, were found. For example, in the fast-FT phenotype, the mutation S112T increased the brightness of both red and blue forms to about the same extent. In the medium-FT phenotype, mutations M143K and L205M increased the brightness of the blue form and increased the efficiency of the blue-to-red chromophore maturation. The introduction of M152L and M152I amino acid substitutions in medium-FT variants substantially increased the brightness of the red but not the blue form. Several mutations such as F63C, S112C and A179V reduced chromophore maturation rates; however, only the latter mutation did not decrease the brightness of the blue form, and therefore we chose this mutation for the slow-FT phenotype.

To make sure that during the multistage screening and selection procedures we did not miss mutants with some advantageous

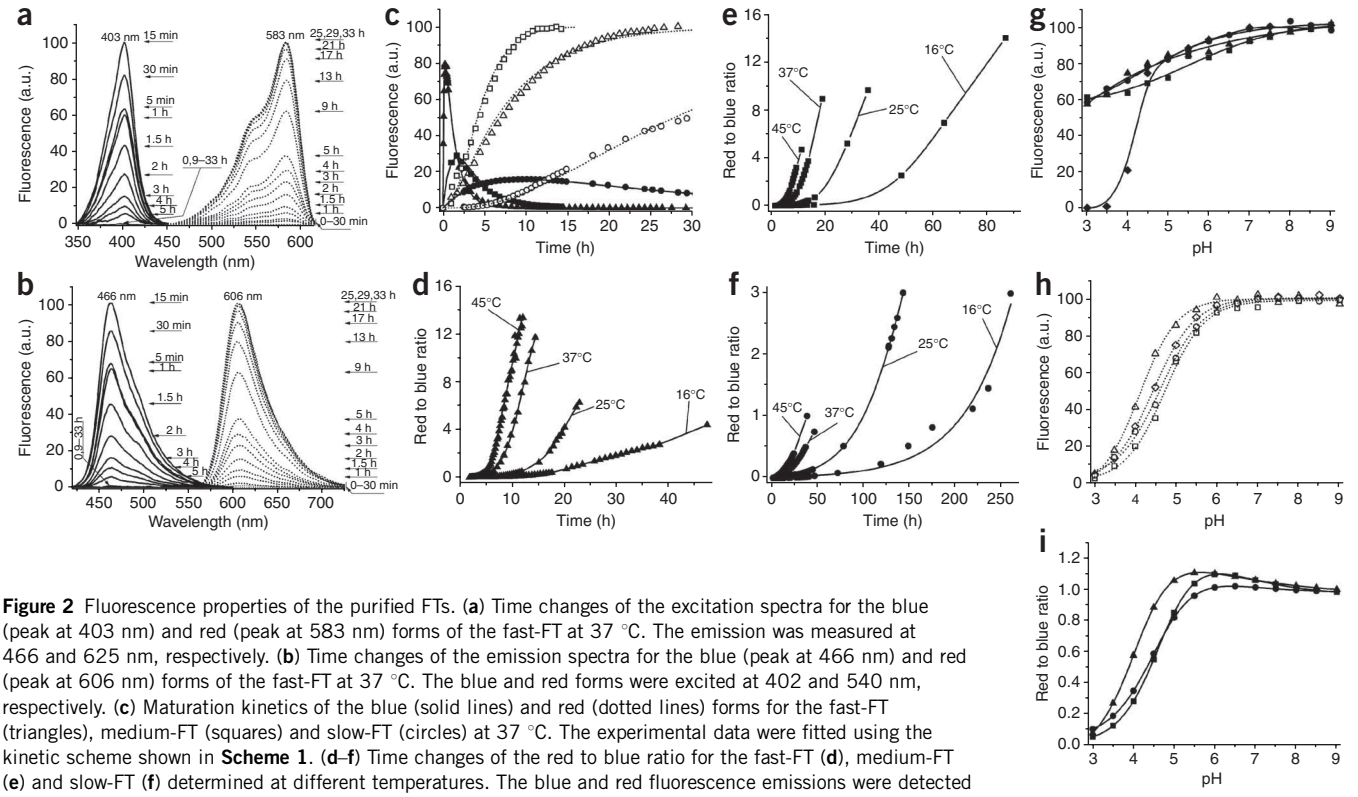

Figure 2 Fluorescence properties of the purified FTs. (**a**) Time changes of the excitation spectra for the blue (peak at 403 nm) and red (peak at 583 nm) forms of the fast-FT at 37 °C. The emission was measured at 466 and 625 nm, respectively. (**b**) Time changes of the emission spectra for the blue (peak at 466 nm) and red (peak at 606 nm) forms of the fast-FT at 37 °C. The blue and red forms were excited at 402 and 540 nm, respectively. (**c**) Maturation kinetics of the blue (solid lines) and red (dotted lines) forms for the fast-FT (triangles), medium-FT (squares) and slow-FT (circles) at 37 °C. The experimental data were fitted using the kinetic scheme shown in **Scheme 1**. (**d**–**f**) Time changes of the red to blue ratio for the fast-FT (**d**), medium-FT (**e**) and slow-FT (**f**) determined at different temperatures. The blue and red fluorescence emissions were detected at 466 nm and 606 nm with excitation at 402 nm and 580 nm, respectively. (**g**–**i**) The pH dependences of the fluorescence intensities of the blue (**g**) and red (**h**) forms and the ratio between the red and blue forms (**i**) for fast-FT (triangles), medium-FT (squares), slow-FT (circles) and EBFP2 (**g**) or mCherry (**h**) (diamonds). The fluorescence for blue and red forms was registered at 466 nm and 606 nm with excitation at 400 nm and 580 nm, respectively. Experimental error is less than 5%.

substitutions at the identified key positions, we applied the best fast-FT, medium-FT and slow-FT variants found in the random mutagenesis for an additional saturated site-specific mutagenesis at positions 69, 84, 143, 179, 203 and 205. However, no better FT versions were found. The final residues neighboring the chromophore in each construct are shown in **Figure 1b–d,** and all important mutations found during the molecular evolution of mCherry into the FTs are summarized in **Supplementary Table 1**.

Properties of FTs *in vitro*

The fluorescence properties of the new constructs were investigated (**Fig. 2**). The blue forms of the purified fast-FT, medium-FT and slow-FT had excitation/emission peaks of 403/466, 401/464 and 402/465 nm, respectively (**Table 1** and **Fig. 2a** for fast-FT; other FTs exhibited similar spectra). The respective red forms had excitation/emission peaks of 583/606, 579/600 and 583/604 nm. The absorbance of both forms had the same maxima as the fluorescence excitation spectra. The external mutations in the FTs were located outside of the dimerizing interfaces observed in the DsRed structure[16]. Subsequently, like the parental mCherry, all FTs exhibited the monomeric behavior (**Supplementary Fig. 2** online).

Molar extinction coefficients and quantum yields of the blue forms of the FTs were in the range of 33,400–49,700 $M^{-1}cm^{-1}$ and 0.30–0.41, respectively (**Table 1**). The fluorescence of the blue forms exhibited high pH stability, with pK_a values below 3.0 (**Fig. 2g**). For comparison, the best blue fluorescent protein reported so far, EBFP2, has lower pH stability, with a pK_a value of about 4.5. Extinction coefficients of the FT red forms were higher than those of the blue forms and varied between 73,100 and 84,200 $M^{-1}cm^{-1}$. The quantum yields for the FT red forms varied in the range of 0.05–0.09. The fluorescences of the red forms had pH stabilities similar to those of the parental mCherry, with pK_a values of 4.1–4.7 (**Fig. 2h**). Because the fluorescence of both blue and red forms decreased with acidification, the ratio between these fluorescence intensities changed with pH notably less than the red signal but more than the blue signal (**Fig. 2i**). For all FTs, the ratio changed less than 8% within the pH range of 5.4–7.4.

During the FT maturation, the fluorescence of the blue forms increased to its maximum value, and after that decreased to zero (**Fig. 2a–c**). The fluorescence of the red forms increased with time with some delay and then reached a plateau. At 37 °C the maxima of the blue fluorescence intensities were observed at 0.25, 1.2 and 9.8 h for the fast-FT, medium-FT and slow-FT, respectively. The half-maxima of the red fluorescence intensities were reached at 7.1, 3.9 and 28 h, respectively, which corresponds to the half-times of the maturation for the red FT forms. These characteristic times increased at lower temperatures such as 16 °C and 25 °C and decreased at higher temperatures such as 45 °C (**Table 1**). The ratios between the red and blue fluorescence intensities exhibited parabolic growth dependencies with time for each FT. The higher the temperature, the faster the growth of the red-to-blue ratio; this observation provided a single meaning for the age of the particular FT (**Fig. 2d–f**). These ratio curves can be easily adapted for other instruments using the ratio of the reference dyes. Furthermore, these data suggest that calibration curves based on the FT red-to-blue ratio can be used to determine the time from the start of FT production under any specific conditions.

Table 1 Properties of the blue and red forms of the purified FTs

Protein		Excitation peak (nm)	Emission peak (nm)	Extinction coefficient (M^{-1} cm^{-1})	Quantum yield	pK_a	Characteristic times (h) 16 °C	25 °C	37 °C	45 °C
Fast-FT	Blue form	403	466	49,700	0.30	2.8	1.6	0.58	0.25	0.18
	Red form	583	606	75,300	0.09	4.1	42	18	7.1	4.2
Medium-FT	Blue form	401	464	44,800	0.41	2.7	2.2	1.6	1.2	0.70
	Red form	579	600	73,100	0.08	4.7	23	8.8	3.9	2.4
Slow-FT	Blue form	402	465	33,400	0.35	2.6	33	20	9.8	7.3
	Red form	583	604	84,200	0.05	4.6	108	69	28	17

Characteristic times correspond to fluorescence maxima for the blue forms, and to maturation half-times for the red forms (**Fig. 2c**).

To quantitatively describe the chromophore conversion pathway in the FTs, we applied kinetic model (1). This model was based on the proposed earlier mechanism for chromophore formation in tetrameric DsRed protein[6]. A spectrally undetectable C-form, which represents a cyclized chromophore-forming tripeptide in the reduced (and therefore colorless) state, is converted into a blue form (B-form), which then turns into a red form (R-form) (**Scheme 1**). It has been shown that in fluorescent proteins, polypeptide folding and cyclization of the chromophore-forming tripeptide occur substantially faster than the oxidation steps[17]. The formation of the B-form precedes the red chromophore formation in many red FPs including DsRed and HcRed1. It has been suggested that the B-form is a common intermediate for the red chromophores[6]. For the FTs, model (1) consisted of the following kinetic steps:

$$C \xrightarrow{k_B} B \xrightarrow{k_I} I \xrightarrow{k_R} R \qquad (1)$$

where C and I are the nonfluorescent chromophore forms, B and R are the blue and red forms of FTs, and k_B, k_I and k_R are the kinetic rate constants[6] (**Scheme 1**). It has been suggested that the B-form is a protonated (neutral) form of the GFP-like chromophore *p*-(hydroxybenzylidene)-imidazolin-5-one[18]. This form results from an oxidation of the Tyr66 αC-βC bond of the C-form with the formation of a double bond. The mature deprotonated (anionic) R-form contains an additional double bond between the α carbon and amide nitrogen of Met65. The I-forms may present an unstable short-lived carbanion intermediate, which is formed from the B-form by a proton abstraction from the α carbon of Met65. The formation of the carbanion intermediate is possible because of stabilization, by a side chain of Arg69 (which is introduced to all FTs by site-specific mutagenesis), of the negative charge delocalized within the aromatic system.

Two steps in the mechanism of red chromophore formation (C→B and I→R) are irreversible because both of them are accompanied by chromophore oxidation with the formation of the double bonds[6,12,16]. The step B→I is the deprotonation of the neutral blue form with formation of at least one intermediate compound, such as the carbanion. Because the exact number and chemical nature of the intermediate compounds is unknown and particularly because the next I→R oxidation step is irreversible, we have approximated the B→I process by irreversible reaction.

We used model (1) above to fit the experimental FT maturation curves obtained *in vitro* for all three purified proteins at 16, 25, 37 and 45 °C (presented in **Fig. 2c** for the fast-FT at 37 °C). We further determined rate constants for each chromophore maturation step in the FTs at different temperatures (**Scheme 1** and **Supplementary Table 2** online). The k_B constants were substantially larger than k_R for the fast-FT and slow-FT, which indicates that the I→R steps were the limiting reactions for red chromophore formation in these FTs. In the case of medium-FT, the limiting step for red form formation was B→I. This suggests that the long-lived intermediate I-form or blue B-form might be responsible for the delays in the formation of the FT red forms—that is, for the timing behavior.

Behavior of FTs in different cell types

To study the behavior of the FTs in a system other than bacteria, we expressed them in stable clones of *Drosophila melanogaster* Schnieder's 2 (S2) cells under the control of the inducible metallothionein promoter[19]. After the induction with copper sulfate of the fast-FT, medium-FT and slow-FT for 0.5, 1 and 2 h, respectively, expression was stopped. The blue and red fluorescence of the S2 cells was then analyzed using flow cytometry at different times during 15 days of cell growth at 25 °C (**Fig. 3**).

To study timing in mammalian cells, the FTs were expressed in the cytoplasm of HeLa cells at 37 °C using the Tet-Off system[20]. Several hours after the transfection, transcription was stopped by addition of a doxycycline, and later the cells were analyzed by flow cytometry at different times (see **Fig. 4a** for slow-FT; other FTs resulted in similar histograms).

As with the purified FTs and the proteins expressed in bacteria, the blue fluorescence of the insect cells at 25 °C and mammalian cells at 37 °C expressing the FTs increased, reached its maxima, and then decreased to almost zero. The red fluorescence also increased with time; however, in contrast to the *in vitro* data, it then slowly decreased (**Fig. 3** and **Fig. 4b**). Furthermore, for all FTs the growth of the blue and red forms and the decrease of the blue forms were slower than those for the purified FTs. These data indicate that (i) the translation

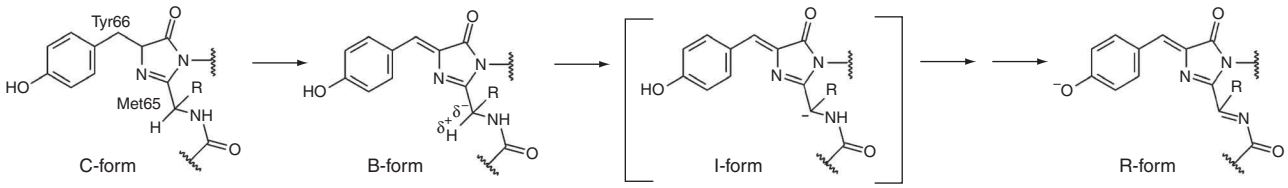

Scheme 1 Suggested transformations of the chemical structures of the chromophore along the red chromophore formation pathway in the FTs.

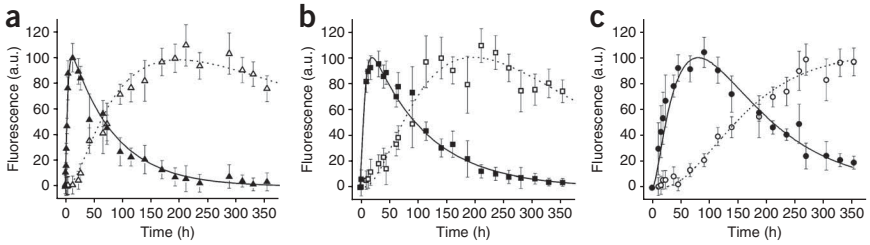

Figure 3 Behavior of the FTs in *D. melanogaster* S2 cells. (**a**–**c**) Time changes of the blue (solid symbols) and red (open symbols) mean fluorescence intensities of the S2 cells stably expressing fast-FT (**a**), medium-FT (**b**) and slow-FT (**c**) at 25 °C determined using flow cytometry. The maxima of the blue fluorescence were achieved at 13 h with fast-FT (**a**), 21 h with medium-FT (**b**) and 80 h with slow-FT (**c**). The maxima of the red fluorescence were achieved at 200 h with fast-FT (**a**) and 197 h with medium-FT (**b**). The experimental data were fitted using the kinetic scheme shown in **Scheme 1**. For all curves the coefficients of determination, R^2, are larger than 0.91. Error bars, s.d.

of FTs occurs for some time after termination of transcription with doxycycline or removal of copper sulfate and (ii) like other proteins, the FTs are susceptible to proteasomal degradation.

To quantitatively describe the kinetics of the blue and red FT forms in live S2 and HeLa cells (**Fig. 3**, **Fig. 4b** and **Supplementary Fig. 3** online), we modified the above model (1) with two minimal additional kinetic steps and got the following kinetic model (2):

$$\mathrm{N} \xrightarrow{k_C} \mathrm{C} \xrightarrow{k_B} \mathrm{B} \xrightarrow{k_I} \mathrm{I} \xrightarrow{k_R} \mathrm{R} \xrightarrow{k_D} \mathrm{D} \qquad (2)$$

where N is ribonucleic acid, D is the degraded nonfluorescent FTs and k_C and k_D are the kinetic rate constants. The first step (from ribonucleic acid to cyclized chromophore-forming tripeptide form) reflects prolongation of protein translation from the ribonucleic acid N after termination of its transcription. The second step (from the red FT to the degraded nonfluorescent FT) reflects degradation of FTs in live cells to the nondetectable D form.

The resulting values of k_C for S2 cells were rather close for all FTs (0.009–0.013 h^{-1}; **Supplementary Table 2**). This was also true for the k_C rate constants in HeLa cells (0.29 h^{-1} for medium-FT and 0.30 h^{-1} for slow-FT), which indicates similar lifetimes for the FT mRNAs in the same type of cells. The k_C values for the HeLa cells suggest that the mRNA amount should be 10% after 8 h and 3% after 12 h incubation with doxycycline. A similar time course for the activity of the luciferase has been observed after inhibition of its transcription with tetracycline[20]. Within 8 h, luciferase activity dropped to about 10% and was less than 2% of its original value after 12 h[20]. The k_D values observed for the FTs at 37 °C were in good agreement with previous reports on the 24 h half-life time for GFP in mammalian cell cytoplasm after the inhibition of its transcription and translation[21].

Intracellular trafficking of LAMP-2A

To explore the advantage of the FTs *in vivo*, we used FTs to study the intracellular trafficking of LAMP-2A. Previous studies on LAMPs trafficking using biochemical and immunofluorescence approaches had suggested that LAMPs can reach the lysosome via two intracellular routes: a direct pathway from the Golgi to the late endosomes and lysosomes[22,23], and an indirect pathway from the Golgi to the plasma membrane following the secretory pathway, and then to lysosomes via endocytosis[24–26]. Although it was initially considered that the pool of LAMPs at the plasma membrane was only evident under certain conditions (such as platelet activation or certain tumors), later studies knocking down adaptor trafficking proteins demonstrated that a portion of cellular LAMPs can be detected at the plasma membrane even under normal physiological conditions (reviewed in ref. 10). In fact, analysis of chimera proteins of the luminal region of LAMP-1 and the three different cytosolic tails of LAMP-2 revealed that the variants reaching the plasma membrane were mainly LAMP-2A and LAMP-2B (ref. 27). However, in most of the previous studies, the plasma membrane location of the LAMPs was analyzed at a steady state. Although the combined use of surface biotinylation and cellular permeabilization helped to demonstrate that some membrane LAMPs are internalized, it was not possible to determine which fraction of the total LAMPs transits through the plasma membrane in a dynamic manner. Lastly, in all the previous studies relying on biochemical analysis, individual differences from cell to cell on the dynamics of internalization of LAMPs from the plasma membrane could not be determined. We predicted that using LAMP-2A–FT fusion proteins, we could possibly estimate the age of the LAMP-2A molecules in different cellular compartments during their trafficking and determine the main LAMP-2A targeting mechanism.

To choose an FT with the appropriate timing behavior, we first tested the localization of LAMP-2A fusion constructs with all FTs expressed under the constitutive cytomegalovirus promoter. Several types of mammalian cells exhibiting different levels of CMA activity were transiently transfected with this construct (see **Supplementary Fig. 4** online for Cos-1 cells). We observed that in the case of LAMP-2A–fast-FT, the blue form mainly localized in an area compatible with the Golgi, and the red form was visualized as vesicular structures (endosomes or lysosomes). The blue form of the LAMP-2A–medium-FT localized in the Golgi, plasma membrane and vesicular structures, and the red form was predominantly detected in the vesicular formations. In the case of the LAMP-2A–slow-FT, the blue form was observed in the vesicular structures, with only a small amount at the cell membrane. All of the red form of the LAMP-2A–slow-FT was observed in the vesicles. Because the LAMP-2A–medium-FT fusion can be detected in several cellular compartments at the same time, this construct was further applied to study trafficking using the Tet-Off system.

We found that at 1 and 6 h after the pulse-chase expression, an early blue form of the LAMP-2A–medium-FT was the major fluorescent form observed in live HeLa Tet-Off cells (**Fig. 4c**). The amount of the blue form then gradually decreased until its complete disappearance at 63 h, whereas the late red form of the LAMP-2A–medium-FT increased, reaching its maximum between 36.5 and 63 h (**Fig. 4c**). The newly synthesized fusion protein was slowly trafficked through the Golgi, where it could be detected for up to 12 h. Between 6 and 21 h, a percentage of the blue form was also observed at the plasma membrane, which, however, was never highlighted with the late red protein. These data indicate that LAMP-2A at the plasma membrane did not result from the fusion of pre-existing lysosomal compartments, but was primarily targeted there from the Golgi after synthesis.

To identify the nature of the vesicular compartments in which LAMP-2A–medium-FT was detected, we applied transferrin-Alexa 488 to visualize early and recycling endosomes, and Lysotracker Green to stain late endosomes and lysosomes (**Supplementary Fig. 5** online). At 6 h after the expression, we observed almost complete co-localization of the late red form of the fusion protein with transferrin-Alexa 488. At 12 and 21 h the co-localization became partial, and

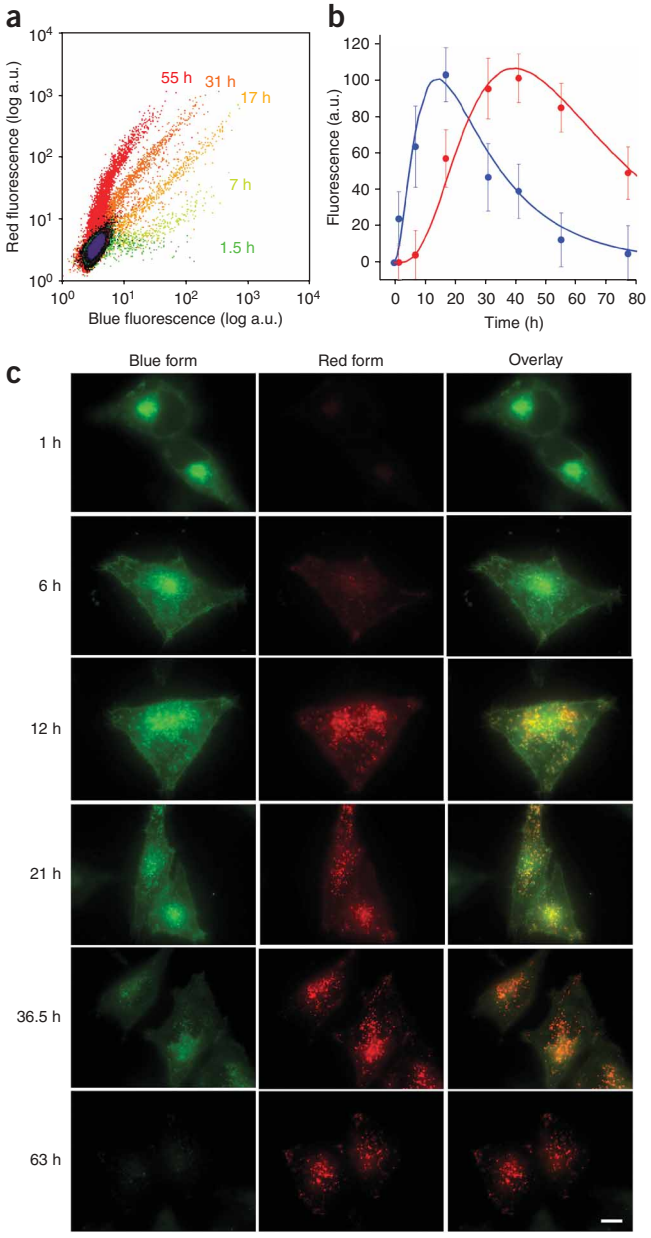

Figure 4 Behavior of the FTs and LAMP-2A–medium-FT fusion protein in mammalian cells. (**a**) HeLa Tet-Off cells transiently expressing slow-FT in cytoplasm were analyzed at different times using flow cytometry. Dot histograms for the selected times such as 1.5 (green), 7 (light green), 17 (yellow), 41 (orange) and 56 (red) hours after the addition of doxycycline are shown. The histogram for the control cells transfected with an empty vector is shown in dark blue. Doxycycline was added 7 h after the transfection. (**b**) Time changes of the blue (blue circles) and red (red circles) mean fluorescence intensities of HeLa Tet-Off cells expressing the slow-FT at 37 °C determined using flow cytometry. The maxima of the blue and red fluorescence intensities were achieved at 17 and 41 h, respectively. The experimental data were fitted using the kinetic scheme shown in **Scheme 1**. The coefficients of determination, R^2, are larger than 0.92. Error bars, s.d. (**c**) Intracellular localization of the LAMP-2A–medium-FT fusion protein in HeLa Tet-Off cells at different time points after the shutting down of transcription with doxycycline. The blue and red forms of LAMP-2A–medium-FT are shown with green and red pseudocolors, respectively. Bar is 10 μm.

only a very small fraction of the LAMP-2A–medium-FT merged with transferrin-Alexa 488 at later times. In contrast, co-localization of the red form with Lysotracker Green was partial at 6 and 12 h, but became almost complete at all times after 21 h.

Because the intense blue fluorescence at the perinuclear region could be masking individual lysosomal structures and thus might complicate discrimination between the different compartments in that region, we also imaged the blue form of LAMP-2A–medium-FT in combination with Lysotracker Green to discriminate between compartments based on a red-to-blue ratio. The regions where blue or red fluorescence was merged with Lysotracker Green were referred to the late endosomes and lysosomes. Bright blue fluorescence was not observed in the regions merged with Lysotracker Green at early times after LAMP-2A–medium-FT expression (**Supplementary Fig. 6** online). The red signal of LAMP-2A–medium-FT in the regions co-stained with Lysotracker Green was substantially larger than that in the perinuclear region. Even when lysosomes identified with Lysotracker staining were occasionally found in the perinuclear region, their red fluorescence was substantially brighter than the red fluorescence in other parts of the perinuclear region that were not stained with Lysotracker.

To determine the nature of the intense blue signal in the perinuclear region observed at earlier times of pulse-chase expression of LAMP-2A–medium-FT, we used β-1,4-galactosyltransferase-EYFP (GalT-EYFP) as a Golgi marker[28–30]. GalT is anchored in the membranes of the *trans*-Golgi network[30–32]. The Golgi marker merged with the intense blue signal localized in the perinuclear region at 1 and 6 h after expression (**Supplementary Fig. 7** online). At later times, the blue signal only coincided partially with GalT-EYFP, whereas co-localization of the red signal with the Golgi marker was not observed at any time after the LAMP-2A expression. These results support the observation that the bright blue fluorescence observed at the perinuclear region corresponds to molecules of LAMP-2A still in the Golgi.

We took advantage of the FT monomeric states to estimate the mean age for the LAMP-2A–medium-FT molecules in different organelles. It is unlikely that a fusion partner such as LAMP-2A affects maturation of the FT chromophore, which is tightly shielded inside of the β-can. Therefore, the same maturation times of blue and red forms of the free FT and FT fusion construct should correspond to the same time after FT expression in both cases. To preserve functionality of the chimera we fused the FTs to the N terminus of LAMP-2A, which is located in the lysosomal lumen. We determined that the red-to-blue ratio for medium-FT had small changes in the pH range of 5.4–7.4 (**Fig. 2i**). This is an important issue because pH values close to 5.4 have been detected in late endosomes and lysosomes, whereas pH values not exceeding 7.4 have been observed in Golgi, early and recycling endosomes, and cytoplasm. These observations allowed us to apply the kinetic model that successfully described spectral changes of the cytoplasmically expressed FTs in live cells. In other words, by comparing the red-to-blue ratios for free medium-FT detected with flow cytometry (**Supplementary Fig. 3**) to those for LAMP-2A–medium-FT obtained using cell imaging (**Fig. 4c**), we have estimated the mean ages of the fusion construct in each of the targeted compartments at various times after its expression has stopped (**Table 2**). The evaluated mean ages in different compartments indicate the indirect intracellular trafficking of LAMP-2A from the Golgi through the plasma membrane and early or recycling endosomes to the late endosomal and lysosomal compartments. 12 h after expression, most of the protein resides in the late endosomes and lysosomes.

Table 2 Behavior of LAMP-2A–medium-FT fusion protein in live HeLa Tet-Off cells

Localization	Time (h)[a]	Relative amount in compartment	Red to blue ratio[b]	Mean age in compartment
Golgi	1	High	0.06 ± 0.02	1.3 h
	6	High	0.07 ± 0.03	1.4 h
	12	Low	n.d.	n.d.
	21	None	n.d.	n.d.
	36.5	None	n.d.	n.d.
	63	None	n.d.	n.d.
Membrane	1	None	n.d.	n.d.
	6	Low	0.08 ± 0.01	1.6 h
	12	Moderate	0.24 ± 0.04	2.6 h
	21	Moderate	0.38 ± 0.05	3.4 h
	36.5	Low	1.28 ± 0.28	6.0 h
	63	None	n.d.	n.d.
Early and recycling endosomes	1	None	n.d.	n.d.
	6	Moderate	0.22 ± 0.05	2.5 h
	12	Moderate	0.43 ± 0.16	3.5 h
	21	Low	1.96 ± 0.65	7.3 h
	36.5	Low	7.0 ± 3.0	12 h
	63	Very low	n.d.	More than 12 h
Late endosomes and lysosomes	1	None	n.d.	n.d.
	6	Low	0.30 ± 0.07	3.0 h
	12	Moderate	0.64 ± 0.36	4.3 h
	21	High	2.0 ± 0.7	7.5 h
	36.5	Very high	61.0 ± 26.0	22 h
	63	High	n.d.	More than 22 h

[a]Time after the addition of doxycycline. [b]Calculations are based on at least 10 cells in each of 2 independent experiments. n.d., red to blue ratio was not determined because there were very low (or no) blue or red fluorescence signals.

DISCUSSION

The primary aim of this investigation was development of new tools to study the spatial and temporal distribution of individual proteins in live cells. As a result of the mutagenesis screening, we have found three monomeric FTs with distinctive blue-to-red conversion timing, which we named fast-FT, medium-FT and slow-FT. The fast-FT has five amino acid mutations as compared to the original mCherry. Among them K69R, L84W and A224S are internal to the β-can mCherry fold and E34K and S151T are external to the fold. The medium-FT exhibits nine amino acid substitutions, of which K69R, L84W, M152I and L205M are internal, and N23D, T43S, Q194L, Y221C and R227H are external. The slow-FT has only four mutations, of which K69R, L84W and A179V are internal and E30V is external. The immediate environment of the chromophores of the FTs is shown in **Figure 1b–d**.

All FTs contain K69R and L84W substitutions. According to the mCherry structure[12], a residue at position 84 influences positioning of residue 69. For example, K84L substitution in mCherry relative to the original DsRed resulted in a 2.7-Å shift of Lys69. Similarly, L84W mutation can lead to a change of position of Arg69 in FTs. On the other hand, the amino acid at position 69 alone plays an important role in formation of the red chromophore. Lysine or arginine amino acids are almost always found at this position in RFPs[14]. In DsRed, K69R is the only substitution that preserved formation of the red chromophore, while slowing its maturation, whereas other substitutions at this position resulted in green chromophores[33]. Therefore Arg69 and Trp84 appear to be the key amino acids responsible for the timing behavior of the mCherry-based blue-to-red FTs.

Other substitutions observed in the FTs are possibly involved in time-tuning of each particular FT. In the mCherry structure, Ala224 forms van der Waals contact with Ile203, which is in close proximity to the chromophore[12]. The A224S substitution in the fast-FT introduces an additional hydroxyl group affecting positioning of Ile203.

Leu205 in mCherry forms several van der Waals contacts with the tyrosine in the chromophore. In addition, Met152 forms van der Waals contacts with Glu150 and Tyr185, which are in close proximity to the chromophore. Therefore, M152I and L205M mutations in the medium-FT can influence red chromophore maturation.

The Ala179 residue in the mCherry structure forms van der Waals contacts with the internal amino acids Met98 and Phe100. However, in the DsRed structure[16], Met98 and Phe100 have van der Waals contacts with Val105. As compared to DsRed, DsRed-E5 FT has only two substitutions, V105A and S203T (ref. 3). Therefore we speculate that the A179V mutation observed in the slow-FT may affect the maturation rate of the red chromophore, much like V105A substitution in DsRed-E5.

In this work we demonstrate the advantages of FTs for visualizing temporal and spatial molecular events using as example the intracellular trafficking of a lysosomal membrane protein. Based on the red-to-blue ratios observed for LAMP-2A–medium-FT in different compartments at various imaging time points, one may suggest the following major intracellular traffic pattern for the protein: Golgi → plasma membrane → early and recycling endosomes → late endosomes and lysosomes. Our data support the predominant indirect targeting of LAMP-2A to lysosomes[11]. The relatively low LAMP-2A levels observed at the plasma membrane suggest a rather short retention time for the protein in this compartment. In fact, at various imaging time points the mean ages of the LAMP-2A–medium-FTs in early and recycling endosomes differ substantially from those in the Golgi (**Table 2**). On the other hand, the difference between the ages of LAMP-2A proteins in the Golgi and those at the plasma membrane is small, which suggests that LAMP-2A is present there for a rather limited time. Therefore, any additional protein flow from the Golgi directly to early and recycling endosomes and then to lysosomes seems to be unlikely.

The use of FTs to study this process has also allowed us to identify a small fraction of LAMP-2A that recycles between endosomes and the plasma membrane. This conclusion is based on the following: if LAMP-2A travels from the Golgi to early endosomes and then recycles between endosomes and the plasma membrane, we should see two populations of endosomes with the different ages of LAMP-2A–FT. The first population would have a red-to-blue ratio smaller than or equal to that on the plasma membrane, while the second population could have a red-to-blue ratio larger than that on the membrane. The microscopy data clearly indicate that for the majority of early and recycling endosomes, the red-to-blue ratio is larger than that on the plasma membrane. However, there is a small fraction (less than 20%) of early and recycling endosomes that have red-to-blue ratios comparable to those on the membrane, but never smaller. Consequently, a quite small fraction of LAMP-2A is involved in the recycling between the plasma membrane and endosomes.

Our results provide, to our knowledge for the first time, an *in vivo* analysis of the spatial and temporal characteristics of a lysosomal membrane protein. Specifically, the FTs allowed us (i) to follow the trafficking of LAMP-2A, (ii) to confirm the universality of the indirect pathway without having to introduce genetic modifications in the adaptor proteins (thus allowing us to avoid possible compensatory

mechanisms), (iii) to establish that engagement of LAMP-2A through the indirect pathway is not a default mechanism, but instead, as proposed through the genetic analysis, affects a large percentage of the intracellular protein and (iv) to estimate the time of trafficking to the plasma membrane and from the membrane to lysosomes in live intact cells, without subjecting the cell membrane to modifications with biotinylation or permeabilization.

The analysis of LAMP-2A behavior demonstrates the advantages of using monomeric FTs to elucidate the dynamics of intracellular proteins under various physiological and pathological conditions. The monomeric FT proteins will also allow for identification of recycling events among compartments, temporal tracking of molecules before and after a particular cellular event (without the need for additional labeling or artificial photoswitching) and timing of particular intracellular post-translational modifications traceable by fluorescent procedures such as ubiquitination and farnesylation. Selection of the appropriate FT is an important step to reveal timing of the specific cellular process to be studied. Therefore, availability of three FTs with distinctive chromophore maturation times will be useful for studies of cellular processes with substantially different time scales. Furthermore, the blue and red fluorescent colors provide the possibility to use FTs together with GFPs for protein multicolor labeling in the cell. The FT monomeric states will be useful for FRET applications with GFP-labeled FRET partners. In contrast to tetrameric DsRed-E5, the monomeric FTs will allow a sequential bimolecular fluorescence complementation of FT molecules followed by FT maturation to determine the intracellular timing of protein-protein interactions[2].

METHODS

Mutagenesis. The gene encoding mCherry was PCR amplified as a *Bgl*II-*Eco*RI fragment and inserted into a pBAD/His-B vector (Invitrogen). Site-specific mutagenesis of the gene encoding mCherry was performed using QuickChange mutagenesis kit (Stratagene). For simultaneous mutagenesis at several positions, an overlap-extension approach was applied[34]. Random mutagenesis was performed with GeneMorph II random mutagenesis kit (Stratagene) using conditions resulting in a mutation frequency of up to 16 mutations per 1,000 base pairs. After mutagenesis, a mixture of the mutants was electroporated into LMG194 bacteria (Invitrogen).

Library screening. To find FTs with distinctive timing behavior, libraries of mutants cloned under the arabinose promoter were screened for bright blue and non-red clones at different times after the induction of protein expression—usually 1, 4 or 24 h for the relatively fast, medium and slow chromophore formation rates, respectively. Then, protein production was suppressed with glucose, and the selected clones were re-screened for the bright red and non-blue phenotype 24 and 48 h later for the fast-medium and the slow maturation rates, respectively. After each round of screening, about 8–10 mutants were considered as promising for the next rounds of mutagenesis; these mutants were characterized by (i) distinctive blue-to-red fluorescence changes, (ii) the brightest fluorescence of both blue and red forms, (iii) specific timing for blue-to-red changes and (iv) external amino acid substitutions that were not located at the dimerizing interfaces observed in the DsRed structure. Further details are described in the **Supplementary Methods** online.

Protein characterization. Maturation of the blue and red forms was studied at 16, 25, 37 and 45 °C in phosphate-buffered saline (PBS). To determine extinction coefficients, we relied on measuring the mature chromophore concentrations[35], taking into account that the extinction coefficient of the model compound of the tyrosine-containing GFP-like chromophores is 44,000 M^{-1} cm^{-1} at 447 nm in 1 M NaOH[35] and about 28,500 M^{-1} cm^{-1} at 382 nm in 1 M HCl[36]. In the case of blue forms, freshly purified proteins were acid-denatured. In the case of red forms, the proteins matured at 37 °C for 24–48 h and afterwards were alkali-denatured. To determine quantum yields, the fluorescence intensities of the blue and red forms were compared with equally absorbing EGFP (quantum yield is 0.60; ref. 37) and mCherry (quantum yield is 0.22; ref. 38), respectively. pH titrations were performed using a series of buffers (100 mM NaOAc, 300 mM NaCl for pH 2.5–5.0, and 100 mM NaH_2PO_4, 300 mM NaCl for pH 4.5–9.0). All fluorescence measurements were performed using a FluoroMax-3 spectrofluorometer (Jobin Yvon). The ratio between the emissions of 0.1 μM rhodamine-101 in 0.01% (w/v) HCl in ethanol at 604 nm (excited at 580 nm) and 10 μM quinine sulfate in 0.1 M H_2SO_4 at 465 nm (excited at 402 nm) under the identical instrumental conditions at 25 °C was 33.7.

Kinetic model for FT maturation. To quantitatively describe the chromophore conversion pathway in the FTs, we considered two kinetic models, (1) and (3). These models were based on the proposed earlier mechanism for the chromophore formation in tetrameric DsRed protein[6]. Model (3) consisted of the following kinetic steps:

$$C \xrightarrow{k_B} B \xrightarrow{k_R} R \qquad (3)$$

Model (1) extends (3) by introducing an intermediate I-form between the B-form and R-form (see above)[6]. We used models (1) and (3) to fit the experimental FT maturation curves obtained *in vitro* for all three purified proteins at 16, 25, 37 and 45 °C using the Gepasi chemical kinetics simulation software[39] with the maximal amount of the red forms accepted as 100%. Model (3) described poorly the experimental data on the kinetics of the maturation of the B-form and R-form in all three FTs. The simulated curves for model (3) had coefficients of determination, R^2, in the range of 0.40–0.62 for the different FTs. The introduction of only a single I-intermediate in model (3) substantially improved the quantitative description of the experimentally observed maturation kinetics for the B-form and R-form. For all three FTs, the simulated curves for model (1) provided R^2 values above 0.99. Therefore we further applied model (1) to describe the kinetic behavior of both the blue and red forms.

To quantitatively describe kinetics of the blue and red FT forms in live S2 and HeLa cells, we used kinetic model (2) (see above). The mean brightnesses for the blue and red forms measured by flow cytometry for the FTs cytoplasmically expressed in S2 and HeLa Tet-Off cells were fitted with kinetic model (2) using the Gepasi software[39]. For fitting, the kinetic constants k_B, k_I and k_R were kept the same as for the purified proteins.

FACS sorting of *D. melanogaster* S2 and HeLa Tet-Off cells. FT expression in the stable S2 pre-clonal cell mixture was induced with 1 mM of $CuSO_4$ for 0.5 h for fast-FT, for 1 h for medium-FT and for 2 h for slow-FT. At specific times after either washing out of $CuSO_4$ (S2) or addition of doxycycline (HeLa), the cells were analyzed with a MoFlo cell sorter using excitation laser lines and emission filters similar to those used for the screening of bacterial libraries.

Microscopy imaging. Imaging of HeLa, Cos-1, NIH3T3 and HeLa Tet-Off cells was performed 13–122 h after transfection. In the case of HeLa Tet-Off cells, doxycycline was added 12 h after the transfection to stop protein expression. Cells were imaged using an Olympus IX81 inverted microscope equipped with a ×100 oil immersion objective lens, with custom blue (390/40 nm exciter, 460/40 nm emitter) and red (570/30 nm exciter, 615/40 nm emitter) filter sets (Chroma), that was operated with SlideBook 4.1 software (Intelligent Imaging Innovations). Because FTs have a tendency to photoconvert from the blue to the red form with high-intensity violet light, which may cause light-induced chromophore maturation, cell images were first acquired in the red channel and then in the blue channel. For quantification of red and blue fluorescence intensities in cellular regions of interest, the background autofluorescence measured in the respective regions of nonfluorescent cells on the same coverslip was usually subtracted.

Note: Supplementary information is available on the Nature Chemical Biology website.

ACKNOWLEDGMENTS

We thank J. Zhang (Albert Einstein College of Medicine) for assistance with flow cytometry. We are grateful to R. Tsien (University of California at San Diego) for the complementary DNA of mCherry and D.Reeves (Albert Einstein College of Medicine) for the pcDNA-3.1-LAMP-2A-TSapphire-GFP vector. This work was

supported by grants from the US National Institutes of Health (GM070358 and GM073913 to V.V.V. and AG021904 to A.M.C.).

AUTHOR CONTRIBUTIONS

F.V.S. and I.S.G. developed the proteins. F.V.S., K.S.M. and K.D.P. characterized the proteins *in vitro*. O.M.S. and F.V.S. characterized the proteins in mammalian cells. V.V.V. designed and planned the project and, together with A.M.C., F.V.S. and O.M.S., wrote the manuscript.

Published online at http://www.nature.com/naturechemicalbiology/
Reprints and permissions information is available online at http://npg.nature.com/reprintsandpermissions/

1. Shaner, N.C., Patterson, G.H. & Davidson, M.W. Advances in fluorescent protein technology. *J. Cell Sci.* **120**, 4247–4260 (2007).
2. Miyawaki, A. & Karasawa, S. Memorizing spatiotemporal patterns. *Nat. Chem. Biol.* **3**, 598–601 (2007).
3. Terskikh, A. *et al.* "Fluorescent timer": protein that changes color with time. *Science* **290**, 1585–1588 (2000).
4. Mirabella, R., Franken, C., van der Krogt, G.N., Bisseling, T. & Geurts, R. Use of the fluorescent timer DsRed-E5 as reporter to monitor dynamics of gene activity in plants. *Plant Physiol.* **135**, 1879–1887 (2004).
5. Duncan, R.R. *et al.* Functional and spatial segregation of secretory vesicle pools according to vesicle age. *Nature* **422**, 176–180 (2003).
6. Verkhusha, V.V., Chudakov, D.M., Gurskaya, N.G., Lukyanov, S. & Lukyanov, K.A. Common pathway for the red chromophore formation in fluorescent proteins and chromoproteins. *Chem. Biol.* **11**, 845–854 (2004).
7. Shaner, N.C. *et al.* Improved monomeric red, orange and yellow fluorescent proteins derived from *Discosoma* sp. red fluorescent protein. *Nat. Biotechnol.* **22**, 1567–1572 (2004).
8. Eskelinen, E. *et al.* Role of LAMP-2 in lysosome biogenesis and autophagy. *Mol. Biol. Cell* **13**, 3355–3368 (2002).
9. Cuervo, A.M. & Dice, J.F. A receptor for the selective uptake and degradation of proteins by lysosomes. *Science* **273**, 501–503 (1996).
10. Bonifacino, J.S. & Traub, L.M. Signals for sorting of transmembrane proteins to endosomes and lysosomes. *Annu. Rev. Biochem.* **72**, 395–447 (2003).
11. Storrie, B. & Desjardins, M. The biogenesis of lysosomes: is it a kiss and run, continuous fusion and fission process? *Bioessays* **18**, 895–903 (1996).
12. Shu, X., Shaner, N.C., Yarbrough, C.A., Tsien, R.Y. & Remington, S.J. Novel chromophores and buried charges control color in mFruits. *Biochemistry* **45**, 9639–9647 (2006).
13. Bevis, B.J. & Glick, B.S. Rapidly maturing variants of the *Discosoma* red fluorescent protein (DsRed). *Nat. Biotechnol.* **20**, 83–87 (2002).
14. Remington, S.J. Fluorescent proteins: maturation, photochemistry and photophysics. *Curr. Opin. Struct. Biol.* **16**, 714–721 (2006).
15. Strongin, D.E. *et al.* Structural rearrangements near the chromophore influence the maturation speed and brightness of DsRed variants. *Protein Eng. Des. Sel.* **20**, 525–534 (2007).
16. Yarbrough, D., Wachter, R.M., Kallio, K., Matz, M.V. & Remington, S.J. Refined crystal structure of DsRed, a red fluorescent protein from coral, at 2.0-A resolution. *Proc. Natl. Acad. Sci. USA* **98**, 462–467 (2001).
17. Reid, B.G. & Flynn, G.C. Chromophore formation in green fluorescent protein. *Biochemistry* **36**, 6786–6791 (1997).
18. Zimmer, M. Green fluorescent protein (GFP): applications, structure, and related photophysical behavior. *Chem. Rev.* **102**, 759–781 (2002).
19. Bunch, T.A., Grinblat, Y. & Goldstein, L.S. Characterization and use of the *Drosophila* metallothionein promoter in cultured *Drosophila* melanogaster cells. *Nucleic Acids Res.* **16**, 1043–1061 (1988).
20. Gossen, M. & Bujard, H. Tight control of gene expression in mammalian cells by tetracycline-responsive promoters. *Proc. Natl. Acad. Sci. USA* **89**, 5547–5551 (1992).
21. Verkhusha, V.V. *et al.* High stability of *Discosoma* DsRed as compared to Aequorea EGFP. *Biochemistry* **42**, 7879–7884 (2003).
22. Harter, C. & Mellman, I. Transport of the lysosomal membrane glycoprotein lgp120 (lgp-A) to lysosomes does not require appearance on the plasma membrane. *J. Cell Biol.* **117**, 311–325 (1992).
23. Hunziker, W. & Geuze, H.J. Intracellular trafficking of lysosomal membrane proteins. *Bioessays* **18**, 379–389 (1996).
24. Carlsson, S.R. & Fukuda, M. The lysosomal membrane glycoprotein lamp-1 is transported to lysosomes by two alternative pathways. *Arch. Biochem. Biophys.* **296**, 630–639 (1992).
25. Mathews, P.M., Martinie, J.B. & Fambrough, D.M. The pathway and targeting signal for delivery of the integral membrane glycoprotein LEP100 to lysosomes. *J. Cell Biol.* **118**, 1027–1040 (1992).
26. Akasaki, K., Michihara, A., Mibuka, K., Fujiwara, Y. & Tsuji, H. Biosynthetic transport of a major lysosomal membrane glycoprotein, lamp-1: convergence of biosynthetic and endocytic pathways occurs at three distinctive points. *Exp. Cell Res.* **220**, 464–473 (1995).
27. Gough, N.R. & Fambrough, D.M. Different steady state subcellular distributions of the three splice variants of lysosome-associated membrane protein LAMP-2 are determined largely by the COOH-terminal amino acid residue. *J. Cell Biol.* **137**, 1161–1169 (1997).
28. Shaper, N.L. *et al.* Bovine galactosyltransferase: identification of a clone by direct immunological screening of a cDNA expression library. *Proc. Natl. Acad. Sci. USA* **83**, 1573–1577 (1986).
29. Narimatsu, H., Sinha, S., Brew, K., Okayama, H. & Qasba, P.K. Cloning and sequencing of cDNA of bovine N-acetylglucosamine (beta 1–4)galactosyltransferase. *Proc. Natl. Acad. Sci. USA* **83**, 4720–4724 (1986).
30. Qasba, P.K., Ramakrishnan, B. & Boeggeman, E. Structure and function of beta -1,4-galactosyltransferase. *Curr. Drug Targets* **9**, 292–309 (2008).
31. Strous, G.J. Golgi and secreted galactosyltransferase. *CRC Crit. Rev. Biochem.* **21**, 119–151 (1986).
32. Teasdale, R.D., D'Agostaro, G. & Gleeson, P.A. The signal for Golgi retention of bovine beta 1,4-galactosyltransferase is in the transmembrane domain. *J. Biol. Chem.* **267**, 4084–4096 (1992).
33. Baird, G.S., Zacharias, D.A. & Tsien, R.Y. Biochemistry, mutagenesis, and oligomerization of DsRed, a red fluorescent protein from coral. *Proc. Natl. Acad. Sci. USA* **97**, 11984–11989 (2000).
34. Ho, S.N., Hunt, H.D., Horton, R.M., Pullen, J.K. & Pease, L.R. Site-directed mutagenesis by overlap extension using the polymerase chain reaction. *Gene* **77**, 51–59 (1989).
35. Chudakov, D.M. *et al.* Photoswitchable cyan fluorescent protein for protein tracking. *Nat. Biotechnol.* **22**, 1435–1439 (2004).
36. Niwa, H. *et al.* Chemical nature of the light emitter of the Aequorea green fluorescent protein. *Proc. Natl. Acad. Sci. USA* **93**, 13617–13622 (1996).
37. Patterson, G.H., Knobel, S.M., Sharif, W.D., Kain, S.R. & Piston, D.W. Use of the green fluorescent protein and its mutants in quantitative fluorescence microscopy. *Biophys. J.* **73**, 2782–2790 (1997).
38. Shaner, N.C., Steinbach, P.A. & Tsien, R.Y. A guide to choosing fluorescent proteins. *Nat. Methods* **2**, 905–909 (2005).
39. Mendes, P. Biochemistry by numbers: simulation of biochemical pathways with Gepasi. *Trends Biochem. Sci.* **22**, 361–363 (1997).